DOI: 10.1002/cmdc.200800346

Exploring the Implications of Vitamin B_{12} Conjugation to Insulin on Insulin Receptor Binding

Amanda K. Petrus,[a] Damian G. Allis,[a] Robert P. Smith,[c] Timothy J. Fairchild,*[b] and Robert P. Doyle*[a]

We recently reported a vitamin B_{12} (B_{12}) based insulin conjugate that produced significantly decreased blood glucose levels in diabetic STZ-rat models. The results of this study posed a fundamental question, namely what implications does B_{12} conjugation have on insulin's interaction with the insulin receptor (IR)? To explore this question we used a combination of molecular dynamics simulations and immunoelectron microscopy, and the results are described herein. This investigation demonstrates that chemical modification of insulin by linking relatively large pendant groups does not inherently interfere with IR recognition. Furthermore, given that we have previously demonstrated a significant drop in blood glucose concentration following the oral administration of the B_{12}–insulin bioconjugate used in this work, it is reasonable to conclude that the IR recognition described herein is associated with maintenance of biological activity for insulin. This outcome offers significant research scope for chemical modification of insulin with the purpose of improving oral-uptake efficiency.

Introduction

The chemical or biological modification of peptides and proteins is commonly employed in the development of therapeutics. The purpose of such modification is to either increase the absorption of such systems via noninvasive routes or extend their biological half-life. A severe constraint of such modification is that the structure of the peptide or protein is ultimately changed, a situation that must not upset the integrity of the structure–function relationship so vital to peptide and protein activity. Insulin is a potential target protein for modification given its importance and widespread administration in the treatment of diabetes. A thriving area of current research for insulin involves the development of an orally administrable form that shows little or no loss of biological activity. Recent work by our group showed that a vitamin B_{12} (B_{12}) based insulin conjugate could produce significantly decreased blood glucose levels in diabetic STZ-rat models.[1] The results of this work inspired us to explore, in vitro, what implications B_{12} conjugation has on insulin's interaction with its receptor. To explore this question we used a combination of molecular dynamics (MD) simulations and immunoelectron microscopy, and the results are described herein.

Upon ingestion, B_{12} first binds to haptocorrin, a salivary enzyme that protects and transports B_{12} through the stomach and into the small intestine. B_{12} then binds to intrinsic factor (IF), a glycosylated protein that transports B_{12} down to the ileum of the small intestine, where the complex binds to the IF–B_{12} receptor on the ileum wall. The IF–B_{12}–receptor complex then undergoes endocytosis, releasing B_{12} into the blood serum, where it is bound to transcobalamin(II) (TCII). When conjugated to insulin, B_{12} must still be recognized for successful serum delivery to occur. Such delivery has been confirmed by the empirical observation of glucose lowering as referenced earlier, accompanied by IF binding assays. Once delivered, the postulated TCII–B_{12}–insulin complex must retain binding affinity with the insulin receptor (IR).

Computational simulations provide predictions for the structures of intermediates and the final TCII–B_{12}–IR complex to consider whether these intermediates meet the structural requirements necessary for cellular uptake. The computational study presented addresses 1) the flexibility of the insulin B chain in solution, 2) the structure of the B_{12}–insulin bioconjugate, 3) the binding of B_{12} and the B_{12}–insulin bioconjugate to TCII, and 4) the binding interaction between the TCII–B_{12}–insulin complex and the IR.

Results and Discussion

The dynamic behavior of insulin in solution and the determination of its binding geometry with the IR have been considered previously.[2–5] The former has been the focus of experimental and computational studies to determine the positions of

[a] *A. K. Petrus, Dr. D. G. Allis, Prof. R. P. Doyle*
Department of Chemistry
Syracuse University, Syracuse, NY 13244 (USA)
Fax: (+1) 315-443-4070
E-mail: rpdoyle@syr.edu

[b] *Prof. T. J. Fairchild*
Department of Exercise Science
Syracuse University, Syracuse, NY 13244 (USA)
Fax: (+1) 315-443-2258
E-mail: tjfairch@syr.edu

[c] *R. P. Smith*
N. C. Brown Center for Ultrastructure Studies, SUNY
College of Environmental Science and Forestry
Syracuse, NY 13210 (USA)

Supporting information for this article is available on the WWW under http://dx.doi.org/10.1002/cmdc.200800346.

amino acid side chains involved in the insulin–IR interaction. More pertinent to the study presented herein, we investigate how the structure of insulin changes in solution to enable it (and the insulin–B_{12}–TCII complex) to bind to the IR. The insulin monomer and structure labels are shown in Figure 1.

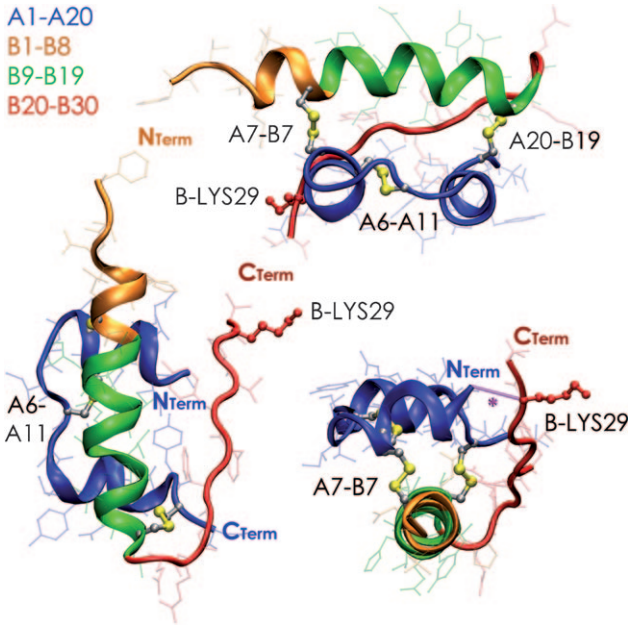

Figure 1. Human insulin monomer from its hexameric crystal form (PDB code: 1AI0). Important regions in the structural and dynamic analysis are differentiated by color. B strand-Lys 29 marks the binding position of the B_{12} bioconjugate. The position of the B29–A1 linkage that yields biologically inactive insulin is marked with an asterisk (lower right).

Insulin is composed of two chains of 21 (A chain) and 30 amino acid residues (B chain) joined by three disulfide linkages (one intra-A/A and two inter-A/B).[6] The α-helical geometry of the A chain (A1–A10 and A12–A20; A-Cys 11 is the non-helical residue involved in the intra-helical disulfide linkage to A-Cys 6) and central B chain segment (B9–B19) are preserved (as determined by NMR[7–9] and MD[10–14] studies) in all physiologically relevant conformations, while the remainder of the B chain (B1–B8 and B20–B30) is marked by significant structural differences between the dimeric/hexameric crystal and various solution-phase forms.

The determined active form of insulin, known as the "T-state" is an open structure, with the B1–B8 conformation restricted by inter-chain hydrogen bonding (B5 to B13) and B20–B30 non-interacting with the IR binding core (A chain and B9–B19). The extended T-state geometry, associated with binding activity and believed to be the dominant form in solution, reveals that the C terminus of the B chain is not significantly involved in the IR binding event. While the closed form ("R-state") of B20–B30 is the form in the dimeric and hexameric crystals of insulin, the ability of this region to unbind from its A/B overlay orientation is critical to the physiological activity of insulin. This is revealed by the absence of insulin activity upon peptide bond formation between B29 and A1 that locks B20–B30 in its crystal orientation.[15]

The structural and dynamic features of the B chain of insulin monomer extend to predictions about the geometry of the B_{12}–insulin bioconjugate, specifically to the flexibility of the B20–B30 region and the retention of insulin binding affinity with the covalently bound B_{12}. The B_{12}–insulin bioconjugate in crystal and extended forms is shown in Figure 2.

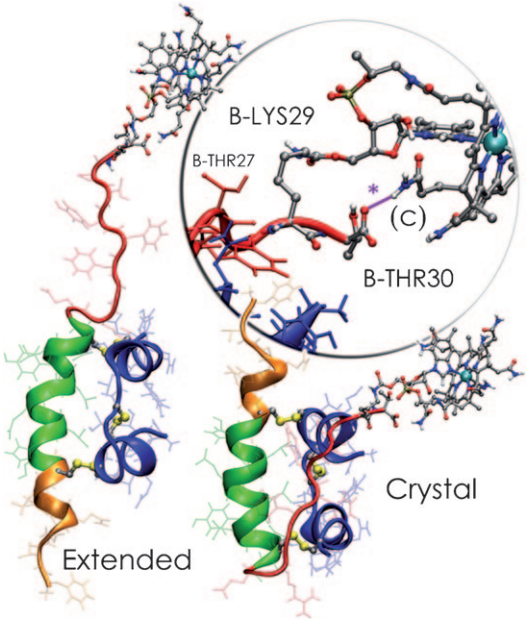

Figure 2. The energy-minimized B_{12}–insulin bioconjugates in extended and crystal forms (relative to the insulin monomer) and the Thr 30-to-amide-(c) hydrogen bond persistent in the MD simulations of both forms. Color schemes for insulin are as indicated in Figure 1.

Simulations (10 ns) of these two forms reveal the same trends in B chain mobility as the unmodified insulin, that is, the insulin A/B binding core geometry is effectively unperturbed by B_{12}. The MD simulations do indicate that the B chain C terminus of insulin (B-Thr 30) is ideally placed to form a hydrogen bond with amide (c) (see Supporting Information). Inspection of the structure indicates that B-Thr 27 is favorably positioned for hydrogen bonding to a phosphate oxygen atom if B-Lys 29 adopts an alternate conformation.

The crystal structure of TCII–B_{12}[15] reveals a great deal about how insulin can be covalently linked to B_{12} without inhibiting its TCII binding. The 1.4 nm solvent-accessible surface of TCII–B_{12} from its crystal structure is shown in Figure 3.

The phosphate and ribose 5′-hydroxy group are two locations that have demonstrated activity retention in bioconjugate studies.[1,16] Both share the same solvent-accessible hole formed by the incomplete TCII encapsulation of B_{12}, and their accessibility even with TCII binding argues that covalently tethered substituents do not significantly alter B_{12} binding, provided these tethers are long enough to avoid steric crowding of the linked substituent and TCII. Numerous additional considerations (such as the persistence of B_{12} binding in the presence

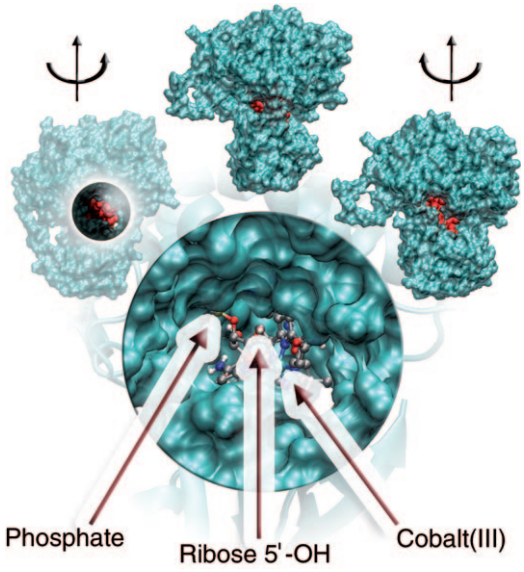

Figure 3. Three views of the 1.4-nm solvent-accessible surface of TCII showing the B_{12} binding position (red). The magnified region shows the positions of the phosphate and the ribose 5′-hydroxy group (at the edge of the solvent surface) and cobalt(III).

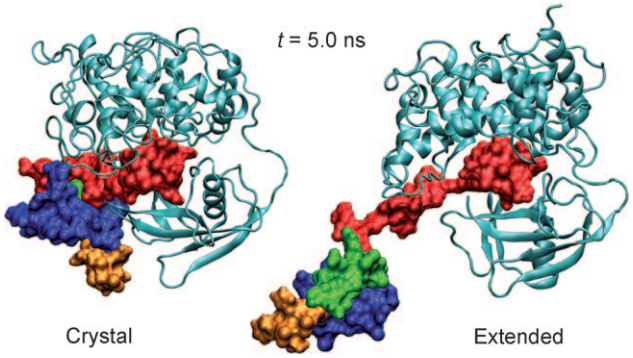

Figure 4. Simulation snapshots (5.0 ns) of the B_{12}–insulin–TCII complex begun from crystal- and extended-geometry insulin (in Figure 2). Both structures are oriented with the corrin ring in the plane of the page. The insulin color scheme is as indicated in Figure 1.

of bulky groups or stronger surface interactions between the substituent and TCII that would attenuate the B_{12} binding interaction strength) need to be addressed before a complete picture can be generated, but the observed accessibility does provide a structural basis for the success of previous bioconjugate studies, as noted elsewhere.[17]

The TCII–B_{12}–insulin complex is considered at two insulin geometries. In the first case, the crystal form of insulin is used as the geometry for the B_{12}–insulin bioconjugate. As the B chain overlays and interacts with the A/B insulin central core in this conformation, this geometry represents what could be considered the most sterically strained B_{12}-bound insulin conformation with respect to the solution-accessible surface of TCII. The second case uses the B_{12}–insulin bioconjugate with the B20–B30 extended, which initially separates the A/B insulin core from TCII by approximately 30 Å. Considering the dynamics of this complex at time scales long enough to identify what might be persistent local geometries or stabilizing surface interactions between insulin and TCII is beyond the scope of the analysis, as the conformational flexibility of the insulin B chain alone has been demonstrated to require considerable modeling timescales to adopt conformations consistent with solution-phase NMR structures. These two forms serve as "limiting cases" to address the persistence of the tethered B_{12} binding within TCII and, specifically in the extended form, how the B chain tether does not affect B_{12} binding. Two snapshots from 10-ns MD simulations of these two conformations are shown in Figure 4.

MD simulations from the insulin crystal geometry do not predict that B_{12} is displaced from its binding pocket. In fact, the simulation indicates that the insulin B chain may adopt a conformation that finds part of the insulin within a cleft on the TCII surface. Longer MD simulations are required to make predictions about the dynamics of these surface interactions. The MD simulation of the insulin extended form also predicts no appreciable change in B_{12} binding in TCII, as expected from the narrower diameter of the peptide tether and the absence of any direct interaction between the insulin core and TCII. The calculations reveal that the B20–B30 tether, in either the crystal or extended forms, provides sufficient length and flexibility to preserve B_{12} binding.

The final complex to consider in this system is the insulin–B_{12}–TCII complex binding with the IR. Here, simulations become considerably more difficult owing to the large size of the overall complex and the long timescales required to allow complete equilibration. The experimental observations become the easier of the two approaches in examining the interaction between TCII and the IR, as the entire complex is sufficiently large to enable direct imaging. The TCII–IR interaction is considered from only the crystal geometries below.

The B_{12}–TCII complex is shown at a position within the IR and oriented such that the solvent-accessible ribose 5′-hydroxy group faces the insulin binding region on the IR in Figure 5. At its crystal structure geometry, the main branches of the dimeric IR structure are separated by 120 Å, tapering to 36 Å at the receptor base. TCII is also tapered in the direction of the B_{12} binding pocket, with an average radius of 46 Å at its widest and approximately 22 Å at the B_{12} binding pocket. Based on comparisons of the crystal structures of these two largest interacting systems in the uptake process, it is identified that TCII can be accommodated within the membrane section of the IR. Combined with the flexibility of the insulin B20–B30 segment, a reasonable description at the molecular level of the uptake process can be drawn from the series of structural analyses.

Given the in vivo activity and computational results, we set out to visualize, in vitro, the conjugate's interaction with the receptor (as well as insulin and B_{12} separately as controls). The RPMI media supplemented with fetal bovine serum (FBS) used has a very low concentration of TCII ($< 9\times10^{-12}$ M), and TCII is in the holo-form due to the presence of B_{12} at concentrations of $\sim 4\times10^{-9}$ M.[18] This ensures no TCII-driven uptake (via possible TCII cell-surface receptors) occurs. T47D breast cancer cells expressing the insulin receptor were used. Post-embedding

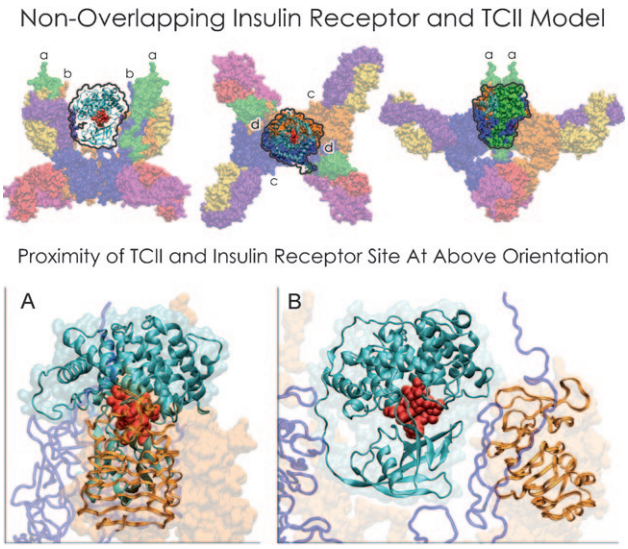

Figure 5. A model of TCII within the IR, with the B_{12} ribose 5′-hydroxy group oriented toward the position of one of the insulin binding sites. In (A), the B_{12} corrin ring is perpendicular to the page; in (B), the corrin ring is in the plane of the page. Approximate distances between symmetry-related (*C*2) positions noted at top in the IR are as follows: a–a = 118 Å, b–b = 68 Å, c–c = 76 Å, d–d = 72 Å.

thin-section immunoelectron microscopy (IEM) was used to assess the location of insulin (12-nm gold beads) and B_{12} (6-nm gold beads) within T47D breast cancer cells (see Figure 6). The 'no-primary' control cells were negative in all sections (data not shown). More than 25 cells were examined ultrastructurally for each of the single labels and for the double IEM. The beads representing the insulin location were almost always in a tight cluster or 'doughnut' shape within the cytoplasm of the cells. The smaller beads representing the location of the B_{12} were more dispersed within each cell examined. For the double label, a close association between insulin and B_{12} was demonstrated almost exclusively. Insulin location, as noted by the gold probe, formed a tight and dense cluster at the cellular membrane consistent with co-localization or "capping" within the plasma membrane (Figure 6A) prior to formation of coated pits and endocytosis (Figure 6B,C). The smaller beads representing B_{12} were interspersed within that cluster or in close proximity to the larger insulin bead. These structures were consistently noted in each of the cells examined, implying specific sites within each cell where insulin aggregated, which is consistent with previous reports.[19] Numerous sectioned cells imaged had a similar pattern with the insulin-representing beads. This tight, specific, and distinctive immunolabeling pattern is likely to represent the co-localization of insulin clustered in lysosomes, as has been previously observed.

The mechanistic foundations for the observed uptake of the B_{12}–insulin bioconjugate are the relative insensitivity of the insulin–IR binding interaction to insulin bulky substituent functionalization on the insulin B chain and the ability of the IR to accommodate the entire TCII–B_{12}–insulin complex in the proposed model.[19]

These results, combined with the known greater affinity of the insulin receptor for insulin (0.12 nM)[20] (as compared with the affinity of the TCII receptor for the TCII–B_{12} complex (0.8 nM)),[18] provide a clearer picture of why a drop in glucose level is obtained when insulin is delivered through the B_{12} pathway in vivo.

Conclusions

This investigation demonstrates that chemical modification of insulin by linking relatively large pendant groups does not interfere with IR recognition. Furthermore, given that we have previously demonstrated a significant drop in blood glucose concentration following the oral administration of this B_{12}–insulin bioconjugate,[1] it is reasonable to conclude that the insulin–IR recognition described herein is associated with maintenance of biological activity for insulin. This outcome offers significant research scope for chemical modification of insulin with the purpose of improving oral-uptake efficiency. Moreover, given that a significant amount of receptor-bound insulin is released from the cell even after endocytosis, the role of conjugation on this process warrants further exploration.

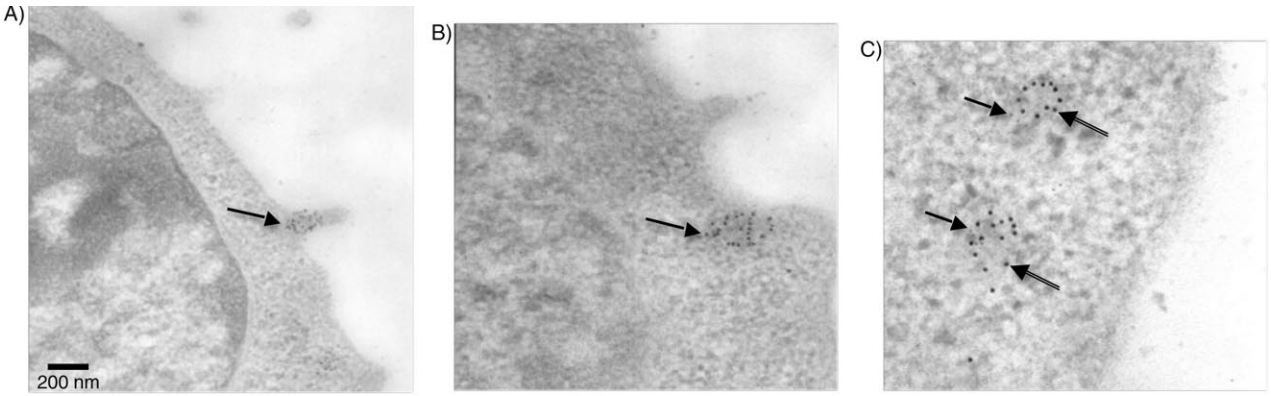

Figure 6. Thin sections of tissue culture cells (T47D) showing A) and B) the conjugate crossing the cellular membrane and becoming internalized (black arrows), and C) co-association of insulin (12-nm beads; ⇒) and B_{12} (6-nm beads; ⟶) at 50000× magnification.

Experimental Section

Vitamin B_{12} (cyanocobalamin), bovine insulin, trifluoroacetic acid (TFA), dimethyl sulfoxide (DMSO), 1,1′-carbonyl-di-(1,2,4-triazole) (CDT), 4-(2-hydroxyethyl)piperazine-1-ethanesulfonic acid (HEPES), Na_2CO_3, dimethylmaleic anhydride (DMMA), Et_2O, EtOH, and sinapinic acid were purchased from Sigma–Aldrich. Intrinsic factor (IF) was purchased from MD Biomedical. DMSO was dried over 4 Å molecular sieves (200–400 mesh, Sigma). Chromatography-grade CH_3CN was purchased from Sigma–Aldrich. The T47D breast cancer cell line was obtained from the American Type Culture Collection (ATCC HTB-133). Fetal bovine serum (FBS) was purchased from Hyclone. RPMI 1640 growth media containing glutamine and phenol red was obtained from Invitrogen. Nonenzymatic cell stripper was purchased from Mediatech. Dialysis tubing (3500 Da cutoff) was purchased from Pierce. H_2O was distilled and deionized (dH_2O) to 18.6 MΩ cm (25 °C) using a Barnstead Nano Diamond ultrapurification machine. HPLC purification was carried out on an Agilent 1100 system with an Eclipse XDB-C_8 column (5 μm, 9.4×250 mm); flow rate: 3 mL min^{-1}. HPLC gradient system: solvent A, 25% CH_3CN/75% dH_2O/0.1% TFA; solvent B, 100% CH_3CN/0.1% TFA; from 0–20 min the gradient went from 100% A to 17% B; from 20–40 min the gradient went from 17→50% B. MALDI-TOF mass spectrometry was performed on a Bruker Autoflex with laser intensity ranging from 35–73%. The MALDI matrix was 10 mg sinapinic acid dissolved in 1 mL mixture of MeOH/CH_3CN (40:60) containing 0.001% TFA. Such spectra were run with and without the presence of 10 mM dithiothreitol (DTT). Insulin was used as control (*m/z*: 5733) to account for variance common with MALDI-TOF mass spectrometry. Electron absorption spectra were used to calculate concentrations were and obtained on a Varian Cary 50 Bio spectrometer in a 1-mL quartz cuvette (Sigma) between 200 nm and 800 nm at 37 °C, regulated with a Peltier instrument. All centrifugation was done at 4000 rpm, at 4 °C for 10 min using a Sorvall centrifuge with swinging rotor (Sorvall Heraeus 75006441 K). All cell work was done in a Labconco Purifier I laminar flow hood that had been disinfected with 70% EtOH and irradiated with UV light.

Bovine insulin (30 mg, 5.23×10^{-6} mol) was obtained from 3 mL of a 10 mg mL^{-1} solution in 25 mM HEPES at pH 8.2. Dimethylmaleic anhydride (6 mg, 4.77×10^{-5} mol) was dissolved in 300 mL DMSO and added to the insulin solution. This solution was then rotated at 4 °C for 30 min, and the solution was adjusted with 1 M $NaHCO_3$ to maintain pH 6.8–7.0. Two more additions of dimethylmaleic anhydride were carried out in an identical fashion. After the final addition, the solution was gently agitated on an orbital shaker overnight at 4 °C. The reaction was then dialyzed against 2 L of 25 mM HEPES buffer (pH 9.7) in snakeskin tubing with a molecular weight cutoff of 3500 Da. Afterward, the pH was checked and adjusted to 9.7 with 1 M Na_2CO_3.

B_{12} (14 mg, 1.05×10^{-5} mol) was treated with 1,1′-carbonyl-di-(1,2,4-triazole) (2 mg, 1.26×10^{-5} mol) in 2 mL dry DMSO at room temperature for 30 min. It was then precipitated in 15 mL Et_2O and collected by centrifugation. The resulting red solid was immediately combined with the insulin solution (pH 9.7) and allowed to rotate in an orbital shaker at 4 °C overnight. The following day the reaction was dialyzed against 5 L dH_2O in snakeskin tubing (3500 Da cutoff). Dialysis against H_2O removes excess B_{12} and lowers the ionic strength of the solution, which aids in chromatographic separation. The dialyzed reaction was then further purified by HPLC.

At a pressure of 91 bar, HPLC yielded a dark red fraction at t_R = 5.26 min, a pink fraction at t_R = 18.48 min, and a series of miniscule pink and clear fractions scattered from t_R = 19.80–23.30 min. MALDI-TOF MS analysis showed the initial red fraction to be B_{12} (~1356 Da), the peak at 18.48 min to be B_{12}–insulin (~7086 Da), and the clear fractions after 19.8 min to be insulin (~5733 Da).

Cell cultures were of the T47D human ductal breast epithelial tumor cell line. They were grown in RPMI 1640 supplemented with 10% FBS at 37 °C. Every three days, the cells were stripped and collected by centrifugation. The cell pellet was then resuspended in 5 mL media; 1 mL of this was passed into 23 mL fresh media. To this, 200 μL bovine insulin (2.0×10^{-5} M) was added after being filtered through a 45-μm filter.

Electron microscopy (EM): Insulin-receptor-containing breast cancer cells (T47D) were incubated with B_{12}–insulin 30 min prior to fixation for EM. Media was decanted from untrypsinized cells and fixed with 4% paraformaldehyde and 0.1% glutaraldehyde in phosphate-buffered saline (PBS) for 30 min. This solution was replaced by fresh fixative for 2 h, at which time cells were gently paddled from the flask with minimal insult. Loose cells were loaded into microfuge tubes and centrifuged to separate the cells and liquid. Here, the fixative was removed and replaced by PBS for 30 min. Cells in tubes were then dehydrated to 90% EtOH, at which time they were gradually infiltrated with LR Gold (London Resin Company, Berkshire, England) at 4 °C over several days. Polymerization of cells in plastic took place under UV light on ice for 24 h. Cells in hardened LR Gold were removed from the microfuge tubes and thin sectioned on a Sorvall MT 6000 ultramicrotome using a diamond knife.

Immunoelectron microscopy (IEM): A post-embedding immunolabeling method was employed. Cells in blocks of LR Gold were sectioned at 60 nm and collected on gold formvar/carbon-coated grids that were immediately processed at room temperature for IEM using a modified procedure developed by Slot and Geuze.[21] Grids with sectioned cells were floated, sections down, on Parafilm containing droplets of the solutions. At the end of each step, excess liquid was removed from the grids with filter paper. Initial blocking of nonspecific sites was accomplished by using a droplet of PBS/BSA and then a droplet of PBS/cold-water fish gelatin (Fluka), 1× 5 min each. Excess aldehyde was quenched using 0.02 M glycine in PBS for 5 min. Grids were then inverted over the first primary antibody for single labeling using anti-insulin, (chicken, H + L) or anti-B_{12} droplets diluted 1:100 in PBS/BSA for 1 h in a humid chamber. A 'no primary' grid was used as a control in each instance. Grids were then rinsed with PBS/BSA (5× 1 min) of PBS/BSA. Insulin was detected by incubation for 1 h with donkey anti-chicken IgY plus IgG (H + L) conjugated to 12-nm colloidal gold beads diluted 1:5 in PBS/BSA (Jackson ImmunoResearch Labs, West Grove, PA, USA). Vitamin B_{12} was detected by incubation for 1 h with donkey anti-rabbit IgG (H + L) conjugated to 6-nm beads. Grids were rinsed (4× 1 min) in PBS and then stabilized with 1% glutaraldehyde in PBS for 5 min. Single-labeled sections of cells were stained and viewed on the transmission electron microscope (TEM) and photographed (see Supporting Information). For double labeling, after rinsing in H_2O, grids were quenched in PBS containing glycine and then the second, primary antibody consisting of anti-vitamin B_{12} was applied. This antibody was diluted 1:100 in PBS/BSA, incubated with sections for 1 h then rinsed with PBS/BSA (5× 1 min) and the second, smaller 6-nm gold tag was applied. Grids were stabilized and rinsed as before, then post-stained sequentially with uranyl acetate and lead citrate. All cells were viewed in a JEOL 2000 TEM operated at 100 kV. Photographic negatives were scanned on a Microtek Scan Master 4 and imported into Adobe Photoshop CS2.

Molecular dynamics (MD) simulations were performed using the program GROMACS (v. 3.3.2)[22] with the GROMOS96[23] (53a6) united-atom force field. All simulations were performed as NPT ensembles with 1.0-fs time-steps and (X,Y,Z) periodic boundary conditions. Simulation temperatures were kept constant at 300 K using Berendsen thermostats[24] with 0.1-ps coupling time constants for solvent (flexible simple point charge (SPC) water model + neutralizing counterions) and solute, separately. Simulation pressures were kept constant using isotropic Berendsen barostats[24] of 1.0 bar with a time coupling constant of 0.5 ps. Electrostatic interactions were evaluated by the particle mesh Ewald (PME) method[25] order 6 with a grid spacing of 0.1 nm in the X,Y,Z directions. The real-space and neighbor-search cutoff were set to 1.2 nm, with nonbonded pair lists updated every 10 steps. The complete set of simulation parameters, GROMOS96 topologies for B_{12}, and energy-minimized structures and solvent box dimensions are provided in the Supporting Information.

Parameter generation, topology definitions, and structural data for B_{12} and the lysine–B_{12} bridge are an amalgam of quantum chemical, crystallographic, and pre-existing G53a6 force-field data. The base structure and heavy atom labeling scheme for the B_{12} topology definition are taken from the human B_{12}–TCII crystal structure (PDB code: 2BB5).[26] The coordination geometry of Co–CN and the Co–N_{corrin} distances were adjusted based on the optimized B_{12} anion (ground-state singlet) structure at an RHF level of theory with the 6-31G(d) basis set[27,28] (which serves as the basis for subsequent RESP calculations as part of a more exhaustive parameterization of B_{12} for the G53a6 force field) using the program Gaussian 03.[29]

The atomic charges and pair exclusion definitions for the B_{12} core (cobalt + corrin ring), as well as the force constants for all bond, angle, and torsion definitions for the Co atom, are based on those in the G53a6 definition for Fe in the heme Fe–porphyrin ring. The combination of Co–N interatomic distances and Fe–N force constants is performed in the interest of computational expediency, with the rationale being that the difference in the stretch and bend terms at the center of the corrin ring are insignificant in the series of simulations, where B_{12} is simply tethered in solution to the insulin B chain or bound within TCII, where numerous H-bonding interactions between functional groups and the protein binding pocket dominate. This approach is extended to CN–B_{12}, where any possible TCII His 173 coordination to the open cobalt site is made impossible by the presence of $[CN]^-$. Angle and torsion definitions assure the proper orientation of aliphatic carbons in the corrin and ribose rings within the united-atom approximation. All remaining (non-sp^3 carbon) hydrogen atoms are defined explicitly in the structure topology (as shown in the Supporting Information). Atomic charge assignments for B_{12} are greatly simplified by the presence of corresponding amino and nucleic acid structural fragments and uncharged aliphatic chains between the functional groups and the corrin ring. The division of B_{12} into amino acid, nucleic acid, and heme subunits used in charge assignments is shown in Figure 1.

Acknowledgements

R.P.D. and T.J.F. acknowledge the Ewing Marion Kauffman Foundation and the Office of the Vice President for Research at Syracuse University for support of this work.

Keywords: bioconjugates · drug delivery · electron microscopy · insulin · receptors

[1] A. K. Petrus, A. R. Vortherms, T. J. Fairchild, R. P. Doyle, *ChemMedChem* **2007**, *2*, 1717.
[2] K. Huang, *J. Mol. Biol.* **2004**, *341*, 529.
[3] M. Lou, T. P. Garrett, N. M. McKern, P. A. Hoyne, V. C. Epa, J. D. Bentley, G. O. Lovrecz, L. J. Cosgrove, M. J. Frenkel, C. W. Ward, *Proc. Natl. Acad. Sci. USA* **2006**, *103*, 12429.
[4] N. M. McKern, *Nature* **2006**, *443*, 218.
[5] C. C. Yip, P. Ottensmeyer, *J. Biol. Chem.* **2003**, *278*, 27329.
[6] X. Chang, A. M. Jorgensen, P. Bardrum, J. J. Led, *Biochemistry* **1997**, *36*, 9409.
[7] F. Y. Dupradeau, T. Richard, G. Le Flem, H. Oulyadi, Y. Prigent, J. P. Monti, *J. Pept. Res.* **2002**, *60*, 56.
[8] B. Hawkins, K. Cross, D. Craik, *Int. J. Pept. Protein Res.* **1995**, *46*, 424.
[9] Q. X. Hua, M. A. Weiss, *Biochemistry* **1991**, *30*, 5505.
[10] M. Falconi, M. T. Cambria, A. Cambria, A. Desideri, *J. Biomol. Struct. Dyn.* **2001**, *18*, 761.
[11] P. Krüger, W. Strassburger, A. Wollmer, W. F. van Gunsteren, G. G. Dodson, *Eur. Biophys. J.* **1987**, *14*, 449.
[12] F. S. Legge, A. Budi, H. Treutlein, I. Yarovsky, *Biophys. Chem.* **2006**, *119*, 146.
[13] A. E. Mark, H. J. Berendsen, W. F. van Gunsteren, *Biochemistry* **1991**, *30*, 10866.
[14] V. Zoete, M. Meuwly, M. Karplus, *J. Mol. Biol.* **2004**, *342*, 913.
[15] U. Derewenda, Z. Derewenda, E. J. Dodson, G. G. Dodson, X. Bing, J. Markussen, *J. Mol. Biol.* **1991**, *220*, 425.
[16] J. F. McEwan, H. S. Veitch, G. J. Russell-Jones, *Bioconjugate Chem.* **1999**, *10*, 1131.
[17] L. Randaccio, S. Geremia, J. Wuerges, *J. Organomet. Chem.* **2007**, *692*, 1198.
[18] T. Amagasaki, R. Green, D. W. Jacobsen, *Blood* **1990**, 76, 1380.
[19] W. C. Duckworth, R. G. Bennett, F. G. Hamel, *Endocr. Rev.* **1998**, *19*, 608.
[20] I. Leconte, C. Auzan, A. Debant, B. Rossi, E. Clauser, *J. Biol. Chem.* **1992**, *267*, 17415.
[21] J. W. Slot, H. J. Geuze, in *Immunolabeling for Electron Microscopy* (Eds.: J. M. Polak, I. M. Varndell), Elsevier BV, Amsterdam, **1984**, 129–142.
[22] D. Van Der Spoel, E. Lindahl, B. Hess, G. Groenhof, A. E. Mark, H. J. Berendsen, *J. Comput. Chem.* **2005**, *26*, 1701.
[23] W. F. van Gunsteren, S. R. Billeter, A. A. Eising, P. H. Hünenberger, P. Krüger, A. E. Mark, W. R. P. Scott, I. G. Tironi, *Biomolecular Simulation: The Gromos 96 Manual and User Guide*, Vdf Hochschulverlag AG, ETH Zürich, **1996**, p. 1044.
[24] H. J. C. Berendsen, J. P. M. Postma, W. F. van Gunsteren, A. DiNola, and J. R. Haak, *J. Chem. Phys.* **1984**, *81*, 3684.
[25] T. Darden, D. York, L. Pedersen, *J. Chem. Phys.* **1993**, *98*, 10089.
[26] J. Wuerges, G. Garau, S. Geremia, S. N. Fedosov, T. E. Petersen, L. Randaccio, *Proc. Natl. Acad. Sci. USA* **2006**, *103*, 4386.
[27] W. J. Hehre, R. Ditchfield, J. A. Pople, *J. Chem. Physics*, **1972**, 56, 2257.
[28] V. A. Rassolov, J. A. Pople, M. A. Ratner, T. L. Windus, *J. Chem. Phys.* **1998**, *109*, 1223.
[29] M. J. Frisch et al., Gaussian 03, Revision C.02, **2004**, Gaussian Inc.: Wallingford, CT (USA).

Received: October 16, 2008
Revised: November 8, 2008
Published online on December 19, 2008

